Magnetization reversal in Py/Gd heterostructures

Pavel N. Lapa,[1,2] Junjia Ding,[1] John E. Pearson,[1] Valentine Novosad,[1] J. S. Jiang,[1] and Axel Hoffmann[1]

[1]*Materials Science Division, Argonne National Laboratory, Argonne, Illinois 60439, USA*

[2]*Department of Physics and Astronomy, Texas A&M University, College Station, Texas 77843-4242, USA*

Using a combination of magnetometry and magnetotransport techniques, we studied temperature and magnetic-field behavior of magnetization in Py/Gd heterostructures. It was shown quantitatively that proximity with Py enhances magnetic order of Gd. Micromagnetic simulations demonstrate that a spin-flop transition observed in a Py/Gd bilayer is due to exchange-spring rotation of magnetization in the Gd layer. Transport measurements show that the magnetoresistance of a [Py (2 nm)/Gd (2 nm)]$_{25}$ multilayer changes sign at the compensation temperature and below 20 K. The positive magnetoresistance above the compensation temperature can be attributed to an in-plane domain wall, which appears because of the structural inhomogeneity of the film over its thickness. By measuring the angular dependence of resistance, we are able to determine the angle between magnetizations in the multilayer and the magnetic field at different temperatures. The measurements reveal that, due to a change in the chemical thickness profile, a noncollinear magnetization configuration is only stable in magnetic fields above 10 kOe.

I. INTRODUCTION

A number of unique phenomena makes surface magnetism of rare-earth Gd an extremely interesting, while immensely challenging, scientific topic. It was shown that, even for a Gd film grown on a nonmagnetic W substrate, magnetic order near the surface can be significantly enhanced [1–4]. When Gd is in proximity with a transition metal (TM), the effect becomes even more prominent [5,6]. For a Fe/Gd multilayer, it was demonstrated that a few atomic monolayers of Gd adjacent to the Fe layer have Curie temperature comparable to that of Fe [7], regardless of the Curie temperature of bulk Gd being only 293 K. Another interesting property of Gd/TM heterostructures is an antiferromagnetic exchange interaction between Gd and TM. This results in magnetizations of adjacent Gd and TM layers being antiparallel to each other without any magnetic fields applied. The unusual antiferromagnetic coupling in combination with the enhancement of magnetic order triggered the use of Gd/TM heterostructures for artificial ferrimagnets applications. As of today, artificial ferrimagnets have been implemented for spin mixing in superconducting spin valves [8], and an out-of-plane anisotropy in Gd/Co [9] and Gd/Fe [10,11] multilayers stimulates the study of the artificial ferrimagnets for a bubble domain application [12–15].

Furthermore, due to the lower ordering temperature of Gd compared to many ferromagnetic TM materials, the magnetization in the Gd layers demonstrates a stronger temperature dependence than the magnetization in the TM layers. For certain Gd/TM heterostructures, at a so-called "compensation temperature", the magnetic moment of the Gd layer becomes equal to the magnetic moment of the TM layer. Because of the antiferromagnetic coupling between the layers, this compensation results in a vanishing total magnetization for these Gd/TM multilayers. Therefore, it is of particular interest to determine magnetization configurations and magnetization reversal mechanisms at the compensation temperature, where magnetic moments of the Gd and TM layers become equal. From a fundamental perspective, Camley and Tilley, using mean-field calculations, showed that a so-called "twisted magnetic state" with a noncollinear configu-

ration of magnetization over the film thickness can appear at the compensation temperature [16]. That is, the magnetization of layers located near the top and bottom surfaces of a film begin to cant, resulting in a well-defined angle with respect to the external magnetic field. As the temperature approaches the compensation temperature, the twists propagate deeper into the multilayer. Camley and Tilley demonstrated that the characteristics of this twisted state strongly depends on the layered structure and its microscopic parameters. The magnetic behavior at the compensation temperature is also interesting due to potential applications. Recently, it was demonstrated that, due to a thermally induced excitation, magnetization of GdFeCo films [17–20] and Gd/Fe [21] artificial ferrimagnets can be switched across the compensation temperature optically, without applying external magnetic field. It is believed that the phenomenon can be used for developing new magnetic recording media [22]. In addition, the antiferromagnetic coupling can result in the formation of interfacial domain walls, which only form and persist for applied magnetic fields exceeding a critical field [23,24].

The anisotropy of polycrystalline Gd and TM [25] causes a hysteretic behavior of magnetization, which drastically complicates the analysis of magnetization reversal in the Gd/TM heterostructures. This complication can be minimized by using Permalloy (Py = $Ni_{0.81}Fe_{0.19}$), which is a TM alloy with very low magnetic anisotropy. Thus, Gd and Py are very promising materials for fabrication of artificial ferrimagnets. Ranchal *et al.* demonstrated that coupling between Gd and Py is antiferromagnetic [26,27], and the intermixing of these materials strongly reduces their coupling energy [28]. Our motivation was to characterize quantitatively the coupling of Gd with Py and magnetic order in these layers, as well as to investigate proximity effects in Py/Gd artificial ferrimagnets.

II. DETAILS OF THE EXPERIMENT AND SIMULATION

Magnetron sputtering at ambient temperatures was used to fabricate three groups of films for this paper. All samples were grown on top of Si/SiO_2 substrates at room temperature.

The deposition rates used for the sputter-deposition of Gd and Py were 1.4 and 0.7 Å/s, respectively. Here, 5-nm-thick Ta layers at the bottom and top of all the films were used as seed and capping layers, respectively. The first group of samples consists of Py (50 nm)/Gd (4 nm) and Py (50 nm)/Au (0.5 nm)/Gd (4 nm) films. These films are designed to determine how proximity with Py influences the magnetization and exchange stiffness of Gd, as well as to evaluate the interlayer coupling between the two metals. The bilayer with a thin Au buffer serves to reveal how interlayer diffusion between Gd and Py affects the strength of the coupling and to show if the coupling can be controlled by placing a thin buffer between Py and Gd. The second group consists of Py/Gd multilayers [Py (t)/Gd $(t)]_{25}$, where t is 1 or 2 nm. The purpose of studying these samples is to determine the mechanism of the magnetization reversal in the vicinity of the compensation temperature. Finally, the third group of samples is designed for estimating the effective exchange stiffness in the Py/Gd multilayers. These samples are composed of a Py/Gd stack adjacent to a 50-nm-thick Py layer, i.e., Py (50 nm)/[Py (t)/Gd $(t)]_{25}$, $t = 1$ or 2 nm. Magnetic moments were measured using a Quantum Design Superconducting Quantum Interference Device (SQUID) magnetometer. Transport measurements were conducted using a conventional four-probe technique; the films were cut into the shape of $9 \times 2\,\mathrm{mm}^2$ stripes. Magnetic field was applied parallel to the films surface. To measure angular dependences of resistance, the stripes were installed on a horizontal rotator. The zero angle corresponds to a position of the stripe in which the current flows in the direction of the external magnetic field. X-ray reflectometry measurements were performed with a Philips diffractometer using Cu Kα (1.54 Å) radiation.

In order to determine the magnetization reversal mechanism and quantitatively evaluate parameters of the Py/Gd films (exchange stiffness, magnetization, and interlayer coupling), the experimental data were simulated using the Object Oriented Micromagnetic Framework (OOMMF) simulation software [29]. Essentially, the micromagnetic model mimics a one-dimensional spin chain directed along the thickness of the film. To imitate an infinite plane, the demagnetization energy term was excluded from the calculation, while magnetization was forced to rotate in plane. Thus, these simulations yield a configuration of spins along the thickness of the films, or rephrasing, they model in-plane domain walls occurring in the films in different magnetic fields. The size of the calculation cell in the direction perpendicular to the film plane was chosen to be 0.25 nm.

III. BILAYER FILMS

To determine the interfacial coupling between Py and Gd and to study how proximity affects magnetic properties of the metals, we prepared the Py (50 nm)/Gd (4 nm) and Py (50 nm)/Au (0.5 nm)/Gd (4 nm) films. The idea behind the design is as follows. Keeping the Gd layer thin allows minimizing the anisotropy energy term, which in turn enables identifying effects of the interfacial interaction more clearly. At the same time, the magnetization of a relatively thick Py layer is predominately along the externally applied magnetic field, thus making the Py layer effectively a "magnetic anchor". The

temperature and magnetic-field dependences of the magnetic moment for the films are compared to those for the reference Py (50 nm) film.

The temperature dependences of the magnetic moment normalized to the film area [Fig. 1(a)] were measured in a small magnetic field (100 Oe) applied parallel to the surface plane. In contrast to a typical rise of magnetization with decreasing temperature demonstrated by the reference Py film, the total magnetic moment of the Py/Gd films (with and without Au) begins to decrease at temperatures below 120 K. This proves that the exchange interaction between Py and Gd is antiferromagnetic. Since the Gd magnetic moment developed at low temperature is antiferromagnetically coupled with that in Py, the total magnetic moment decreases. Importantly, the magnetic moments of the Py/Gd samples are lower than the magnetic moment of the reference Py (50 nm) film even at temperatures above 120 K. We assume that, due to proximity, a part of the Gd layer immediately adjacent to Py has a Curie temperature higher that the rest of the Gd layer. This part of the Gd layer remains ferromagnetic at higher temperatures, which reduces the magnetic moment of the Py/Gd films in comparison to the reference single-layer Py film even at temperatures above 120 K.

Magnetization curves of the Py (50 nm)/Gd (4 nm) and Py (50 nm)/Au (0.5 nm)/Gd (4 nm) films [Fig. 1(b)] demonstrate another interesting effect previously reported for Gd/Fe [30–32], Gd/Ni [5], and Gd/Co [33,34] films, which is usually called a "spin-flop transition". Namely, at a critical field $H_{\mathrm{CR}} = 1.3\,\mathrm{kOe}$ for the Py (50 nm)/Gd (4 nm) film, the magnetic moment exhibits a fast nonlinear growth. Basically, in order to minimize the Zeeman energy, it becomes energetically favorable for the magnetization in the Gd layer to rotate so that it becomes aligned along the magnetic field. The microscopic mechanism of this rotation can be quite complicated, and it strongly depends on the microscopic parameters of the metals. First, let us assume that the exchange stiffness of Gd and Py is high (rigid-spin approximation) and the interfacial coupling is weak in comparison to the interatomic coupling in these materials. In this case, the spin-flop is realized by a coherent rotation of the magnetization in the entire Gd layer with respect to the magnetization in the Py layer. Micromagnetic simulations show that, under the assumption of the rigid-spin approximation, the total magnetization would demonstrate a linear rise with the magnetic field above H_{CR}, followed by a saturation. However, the curves in Fig. 1(b) demonstrate a different behavior: the magnetization grows nonlinearly, and the full saturation is not achieved even in high magnetic fields (40 kOe). It means that the assumption about the "weak" interface is unjustified for the system, and the switching at H_{CR} does not happen due to the coherent rotation of Py and Gd magnetization with respect to each other. Another important feature of the magnetization curves which the rigid-spin approximation fails to explain is the almost linear rise of the magnetization with magnetic fields below H_{CR} [inset in Fig. 1(b)].

It is clear that finite values of the exchange stiffness of Gd and Py must be taken into account for an adequate modeling of the magnetic reversal in the Py/Gd bilayer. Importantly, microscopic properties of materials at the Py/Gd interface are defined by two counteractive processes. On one hand, because the materials have different Curie temperatures, proximity
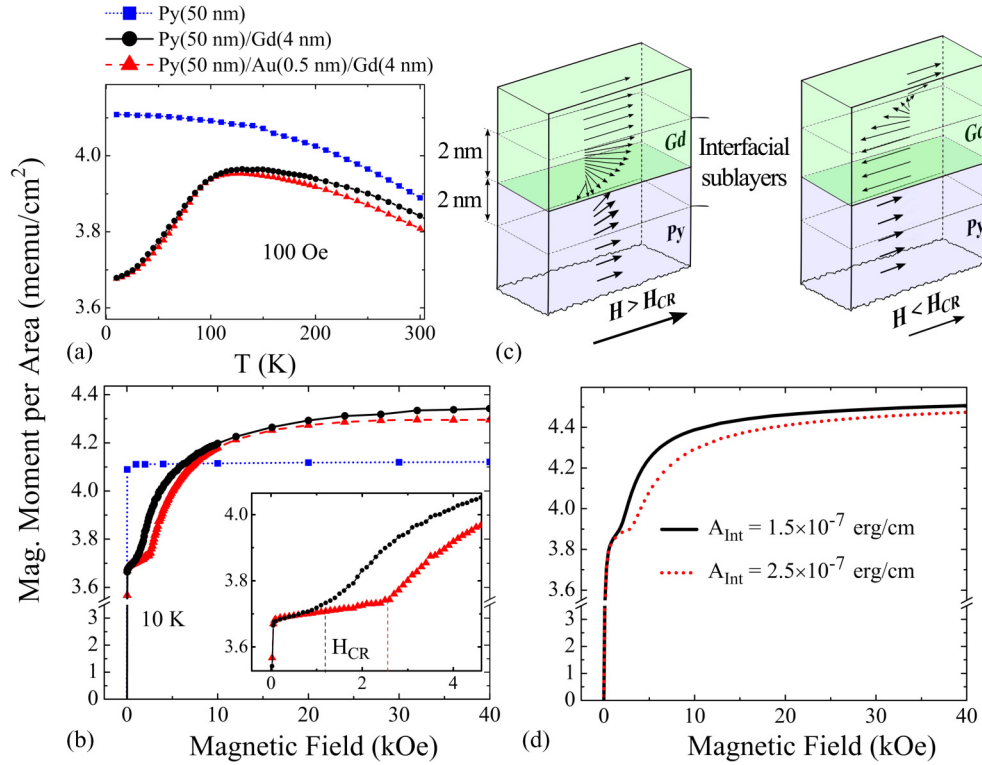
FIG. 1. (a) Temperature dependences of the magnetic moment per area for the Py (50 nm), Py (50 nm)/Gd (4 nm), and Py (50 nm)/Au (0.5 nm)/Gd (4 nm) films measured at a 100 Oe magnetic field. (b) Magnetization curves of these films measured at 10 K. (c) Schematics of exchange springs in the Py/Gd film above and below H_{CR}. (d) Micromagnetic simulations of the magnetization curves for the Py/Gd films. Exchange stiffness (A_{Int}) of the interfacial sublayers was varied to simulate reversals for the Py/Gd bilayers with ($A_{Int} = 1.5 \times 10^{-7}$ erg/cm) and without the Au buffer ($A_{Int} = 2.5 \times 10^{-7}$ erg/cm).

is responsible for the reduction of the exchange stiffness in a thin Py sublayer adjacent to the interface A_{Py_Int} and the enhancement of that in a thin Gd sublayer adjacent to the interface A_{Gd_Int}. On the other hand, intermixing of Py and Gd [5,35] results in adding Ni to Gd, which strongly reduces the Curie temperature of the latter [28,36]. This in turn is attributed to the suppression of A_{Gd_Int} and A_{Py_Int}. Based on the temperature and magnetic-field dependences of the magnetization, we propose the following micromagnetic model to simulate the experimental data for the Py/Gd bilayer. At low temperatures, the exchange stiffness of a 2-nm-thick Gd sublayer and a 2-nm-thick sublayer of Py adjacent to the interface [Fig. 1(c)] is relatively low ($A_{Gd\_Int} = A_{Py\_Int} = A_{Int} = 1.5 \times 10^{-7}$ erg/cm). Due to the low stiffness, the magnetizations in these interfacial Gd and Py sublayers begin to twist along the field at H_{CR}. A micromagnetic simulation [Fig. 1(d)] shows this twist causes a nonlinear rise of the magnetization when the magnetic field is increased above H_{CR}, and the full saturation is not achieved even in high magnetic fields, which is in agreement with the experimental data. The proposed micromagnetic model is also capable of explaining the linear rise of magnetization for the magnetic field below H_{CR} [inset in Fig. 1(b)]. Indeed, if the magnetic order in the top part of the Gd layer is extremely reduced, e.g., its exchange stiffness A_{Gd_Top} is of the order of 1.5×10^{-9} erg/cm, then the magnetization in the top Gd sublayer aligns with the magnetic field, whereas the magnetization in the bottom interfacial Gd sublayer is directed opposite to the field. The simulation shows that this transition

of spins from parallel to antiparallel-to-magnetic-field states is realized through another magnetization twist within the Gd layer. This twist yields a modest rise of magnetization in low magnetic fields [Fig. 1(d)]. The micromagnetic parameters used for the simulation are: $M_{Py} = 810$ emu/cm^3, $A_{Py} = 10 \times 10^{-7}$ erg/cm; M_{Gd} is 1800 emu/cm^3 and 1000 emu/cm^3 for the bottom (interfacial) and top Gd sublayers, respectively; $A_{Int} = 1.5 \times 10^{-7}$ erg/cm, $A_{Gd\_Top} = 1.5 \times 10^{-9}$ erg/cm; exchange stiffness through the Py-Gd interface (A_{Py-Gd}) is 1.5×10^{-7} erg/cm.

The strong reduction of the exchange stiffness in the top part of the Gd layer may happen for a number of reasons. First, roughness and intermixing of Gd with the Ta layer, which was used for capping, can result in a formation of a sublayer with reduced magnetic interactions. Due to the strong localization of the $4f$ electrons responsible for the magnetic moment of Gd, the presence of Ta does not strongly suppress the magnetization of this Gd sublayer; however, it may strongly affect the Gd-Gd distance, causing reduction of the exchange coupling in the top part of the Gd layer. Second, the Ta atoms may modify hybridization between the $4f$ and conduction electrons, which potentially can result in small A_{Gd_Top}. There is no evidence, however, that these mechanisms can provide such a significant suppression of exchange stiffness. Thus, small A_{Gd_Top} must be considered as one of the assumptions, which enable explaining the behavior of the magnetization curve in the magnetic fields below H_{CR}. As an alternative mechanism of this behavior, it can be assumed that the Ta layer can produce a strain in the top

Gd sublayer. Due to magnetostriction of Gd, the strain causes enhancement of the Gd magnetic anisotropy, which yields the viscous behavior in the low magnetic fields. However, the micromagnetic simulations showed that too strong a change in Gd magnetic anisotropy would be required for realization of this mechanism.

It was shown that the interfacial exchange coupling between Py and Gd can be controlled by inserting an ultrathin buffer between Gd and TM which blocks intermixing [37]. To determine how the stiffness of the interfacial exchange spring and, hence, H_{CR} is affected by a buffer layer, we inserted a 0.5-nm-thick Au buffer between Py and Gd. The first effect of the buffer is that the total magnetic moment at temperatures above 170 K becomes lower than that for the bilayer without Au [Fig. 1(a)]. This means that due to the reduction of the intermixing, a thicker part of the Gd layer is ferromagnetic at higher temperatures. Therefore, the drop of the total magnetic moment due to the antiferromagnetic alignment of Gd and Py is more substantial. Second, H_{CR} for the Py (50 nm)/Au (0.5 nm)/Gd (4 nm) trilayer is 2.4 kOe, which is almost twice as large as H_{CR} for the Py/Gd bilayer (1.3 kOe). From these observations, we draw three conclusions. First, the increase in H_{CR} for the bilayer with the Au layer proves that the interface by itself is not a "weak link" of the coupling; otherwise, the presence of the Au layer would lead to a reduction of the coupling and H_{CR}. Second, the coupling is defined by the exchange stiffness A_{Int} of the Py and Gd interfacial sublayers, which is strongly affected by the intermixing. Third, the intermixing between Py and Gd and, hence, the effective coupling can be controlled by placing an ultrathin conducting buffer layer between the metals. Our micromagnetic model is capable of fitting magnetization curves for both samples, with and without the Au buffer. The only parameter that must be adjusted is A_{Int}. Here, $A_{Int} = 2.5 \times 10^{-7}$ erg/cm provides a good fit of the experimental magnetization curve for the Py (50 nm)/Au (0.5 nm)/Gd (4 nm) film [Fig. 1(d)].

IV. MULTILAYER FILMS

In the micromagnetic model for the bilayers, to account for the change in the exchange stiffness of the Py and Gd near the interface due to proximity effect, the 2-nm-thick sublayers were introduced on each side of the Py/Gd interface [Fig. 1(c)]. Interdiffusion of Gd and Py was neglected in the model. To determine how the intermixing influences the magnetic properties of an artificial Py/Gd ferrimagnet and to improve the micromagnetic model proposed for explaining the magnetization reversal process in the Py/Gd bilayers, we studied magnetic and magnetotransport properties of the [Py (1 nm)/Gd (1 nm)]$_{25}$ and [Py (2 nm)/Gd (2 nm)]$_{25}$ multilayers over a wide range of temperatures and magnetic fields. The temperature dependences of the magnetization for these samples measured in a small magnetic field (100 Oe) are shown in Fig. 2(a). The [Py (1 nm)/Gd (1 nm)]$_{25}$ film becomes ferromagnetic only at temperatures below 275 K [Fig. 2(a) open circles]. This temperature is below the Curie temperatures for bulk Py (850 K) and Gd (292 K). The absence of a clear compensation temperature and the reduced ordering temperature for the thinner Py and Gd layers
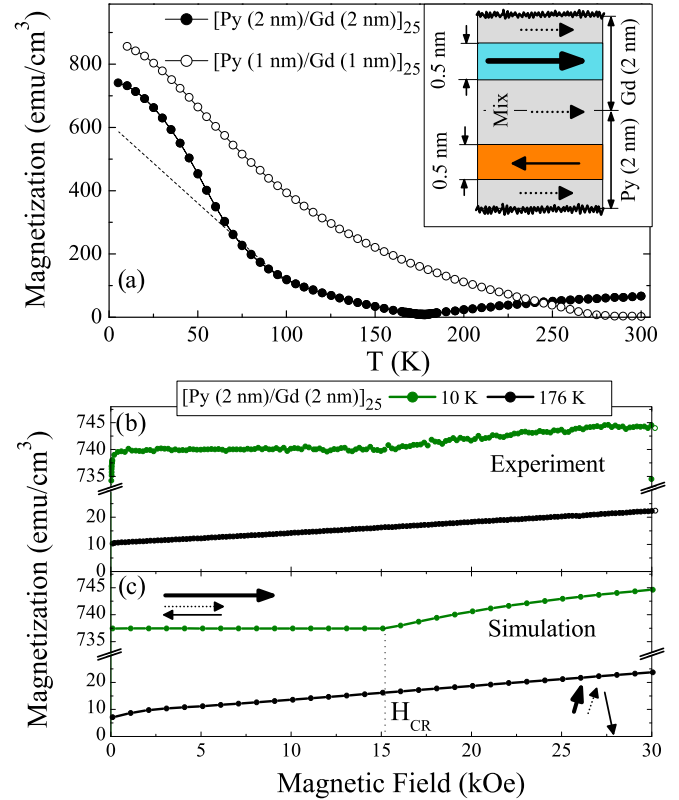

FIG. 2. (a) Temperature dependences of the magnetization for the [Py (1 nm)/Gd (1 nm)]$_{25}$ film (open circles) and [Py (2 nm)/Gd (2 nm)]$_{25}$ (solid circles) films; a dotted line is drawn to illustrate the contribution of the Gd-core sublayers to the total magnetization; schematic in the right upper corner illustrates material distribution and positions of the Py-core (orange) and Gd-core (blue) magnetic sublayers in the [Py (2 nm)/Gd (2 nm)]$_{25}$ film. (b) Experimental and (c) simulated magnetization curves for the [Py (2 nm)/Gd (2 nm)]$_{25}$ film at 10 K (green) and at the compensation temperature (black). Arrows illustrate the direction of magnetizations in the Py-core (thin solid arrow), Gd-core (thick solid arrow), and Mix (dashed arrow) sublayers. The insets at the upper-left and bottom-right corners of (c) illustrate magnetization configurations at 10 and 176 K, respectively.

suggest that the intermixing is a substantial issue for this multilayer sample. Basically, the intermixing is so significant that, in the first approximation, it can be assumed that the entire [Py (1 nm)/Gd (1 nm)]$_{25}$ film is composed of a PyGd alloy. This observation is confirmed by an x-ray reflectivity measurement (Fig. 3). It is seen that comparatively high superlattice fringes appear only for the film with 2-nm-thick layers.

Even though the [Py (1 nm)/Gd (1 nm)]$_{25}$ film is completely intermixed, the magnetic moment of Gd is aligned antiparallel to the magnetic moments of Ni and Fe. At 10 K, the magnetic moment of Gd exceeds the aggregated magnetic moment of Ni and Fe, and hence, the Gd magnetic moment is along the magnetic field at low temperatures. At the same time, the absence of the compensation indicates that the magnetic moment of Gd grows coherently with the aggregated magnetic moment of Ni and Fe. Thus, it can be concluded that the alignment of the Gd magnetic moment along the magnetic field
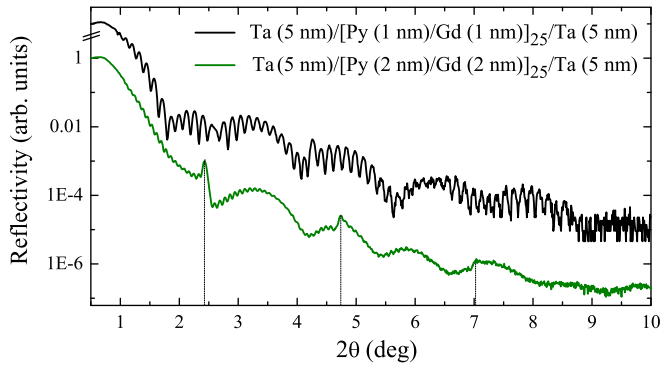
FIG. 3. X-ray reflectivity curves for the [Py (1 nm)/Gd (1 nm)]$_{25}$ (black line) and [Py (2 nm)/Gd (2 nm)]$_{25}$ (green line) films. Short-dashed lines illustrate the positions of the superlattice fringes for the latter film.

in the PyGd alloy is preserved in the 10–275 K temperature range.

Since the layers of the [Py (2 nm)/Gd (2 nm)]$_{25}$ film are not completely intermixed, the film demonstrates a more complex, ferrimagneticlike, temperature dependence of the magnetization [Fig. 2(a) solid circles]. The magnetization of this multilayer is low (70 emu/cm^3) at 300 K. Most likely, this magnetization is due to thin core parts of the Py layers which are not affected by the intermixing of Py and Gd [inset Fig. 2(a)]. At high temperatures, the magnetization in these core sublayers of Py is aligned along the magnetic field. While the film is cooled down, the magnetization of the mixed interfacial regions of Py and Gd (denoted "Mix" further in the text) starts to grow. If we assume that the composition of the Mix sublayers is identical to the composition of the PyGd alloy consisting of the [Py (1 nm)/Gd (1 nm)]$_{25}$ film, then for these Mix sublayers, the magnetic moment of Gd exceeds the magnetic moments of Fe and Ni in the 10–275 K temperature range. Hence, the total magnetic moment of the Mix sublayers tends to align opposite to the magnetic moment in the Py-core sublayers. This leads to a decrease in the total magnetization. At the compensation temperature of 176 K, the magnetic moment of the Py-core sublayers is equal to the magnetic moment of the mixed sublayers, resulting in almost zero magnetization (8 emu/cm^3) of the multilayer at 176 K. Below the compensation temperature, the magnetic moment of the Mix sublayers becomes higher than the moment of the Py-core sublayers; hence, the magnetization is Gd-aligned at these temperatures. Importantly, in contrast to the [Py (1 nm)/Gd (1 nm)]$_{25}$ multilayer, the magnetization begins to rise strongly at temperatures below 75 K. We consider that, similarly to the Py-core sublayers, the core parts of the Gd layers are not affected by the intermixing. The rise of the magnetization in these Gd-core sublayers below 75 K causes the upturn of the total magnetization. By taking into account the values of magnetization at 300 and 10 K and assuming that the temperature dependence of the magnetization for the Mix sublayers coincides with that for the [Py (1 nm)/Gd (1 nm)]$_{25}$ film, it was estimated that the effective thicknesses of the Py- and Gd-core sublayers are about 0.5 nm, wherein the rest of the multilayer is filled with the PyGd alloy [inset in Fig. 2(a)].

Our magnetometry measurements show that, for both [Py (2 nm)/Gd (2 nm)]$_{25}$ and [Py (1 nm)/Gd (1 nm)]$_{25}$ films, the coercive field does not exceed 10 Oe in the 10–200 K temperature range. This means that the anisotropy of these films is comparable with that for Py, which makes them a good choice for application as a soft artificial ferrimagnet. Noteworthy, the study also showed that the anisotropy becomes significantly higher if the thickness of the Gd layers increases.

The magnetization curves of the [Py (2 nm)/Gd (2 nm)]$_{25}$ multilayer measured at 10 K (green dots) and at the compensation temperature (black dots) are shown in Fig. 2(b). Importantly, even at the compensation temperature, the magnetization of the film is not zero. Furthermore, the magnetization curve does not pass through the origin in zero magnetic field. At the compensation temperature, the magnetization rises linearly in magnetic fields up to 70 kOe, whereas at 10 K, a complete saturation of magnetization is achieved already in a very small magnetic field (below 50 Oe). We also observe that, at 10 K, the magnetization experiences a rise at a magnetic field of 16 kOe [Fig. 2(b)], similarly to the one demonstrated by the PyGd bilayers [Fig. 1(b)]. Knowing the estimated thicknesses of the Py- and Gd-core sublayers [inset in Fig. 2(a)], we modeled the magnetization curves of the [Py (2 nm)/Gd (2 nm)]$_{25}$ multilayer micromagnetically. Figure 2(c) presents simulated magnetization curves obtained for 10 K (green line) and 176 K (black line). Micromagnetic parameters used for the simulation are $A_{\mathrm{Mix}} = A_{\mathrm{Py}} = 1.5 \times 10^{-7}$ erg/cm, $M_{\mathrm{Py}} = 810$ emu/cm^3. For $T = 10$ K, $A_{\mathrm{Gd}} = 1.5 \times 10^{-7}$ erg/cm, $M_{\mathrm{Mix}} = 861$ emu/cm^3, $M_{\mathrm{Gd}} = 1600$ emu/cm^3, $M_{\mathrm{Py}} = 810$ emu/cm^3. Based on the fact that the Gd-core sublayers gain significant magnetic moment only below 75 K, we assume that the exchange stiffness and magnetization of the Gd-core sublayers are highly suppressed at 176 K, i.e., $A_{\mathrm{Gd}} = 0.1 \times 10^{-7}$ erg/cm, $M_{\mathrm{Gd}} = M_{\mathrm{Mix}} = 116$ emu/cm^3. The simulations of the magnetization reversal at 10 K show that, in a magnetic field below 15.5 kOe, the magnetizations of the Gd-core and Mix sublayers are pointed along the magnetic field, while the magnetizations in the Py-core sublayers are opposite to the field. Because the very bottom Py layer and the very top Gd layer are adjacent to only one Gd and Py layer, respectively, their structure is different from that of the other layers in the [Py (2 nm)/Gd (2 nm)]$_{25}$ multilayer. Namely, these layers are subjected to intermixing only from one side, and hence, the thicknesses of the corresponding Py- and Gd-core sublayers in these layers are 1.25 nm instead 0.5 nm. The simulations show that, at 10 K, when the magnetic field exceeds $H_{\mathrm{CR}} = 15.5$ kOe, the magnetization in the very first Py layer rotates to align along the magnetic field. This yields an exchange-spring twist of the magnetization near the bottom surface of the film similarly to the one observed in the PyGd bilayers. The rest of the film preserves antiparallel magnetization alignment along the magnetic field. In order to minimize the total energy at 176 K, when the magnetic moment of the Gd-core/Mix sublayers compensates that of the Py-core sublayers, the corresponding magnetizations tend to align perpendicular to the magnetic field, at the same time, being almost antiparallel to each other (noncollinear configuration). Again, since the magnetic structure of the very bottom Py and the very top Gd layers is different from the structure of the layers in the depth of the film, the symmetry of the magnetic

(a)

(b)

[Py (2 nm)/Gd (2 nm)]$_{25}$ —— longitudinal —— transverse

(c)

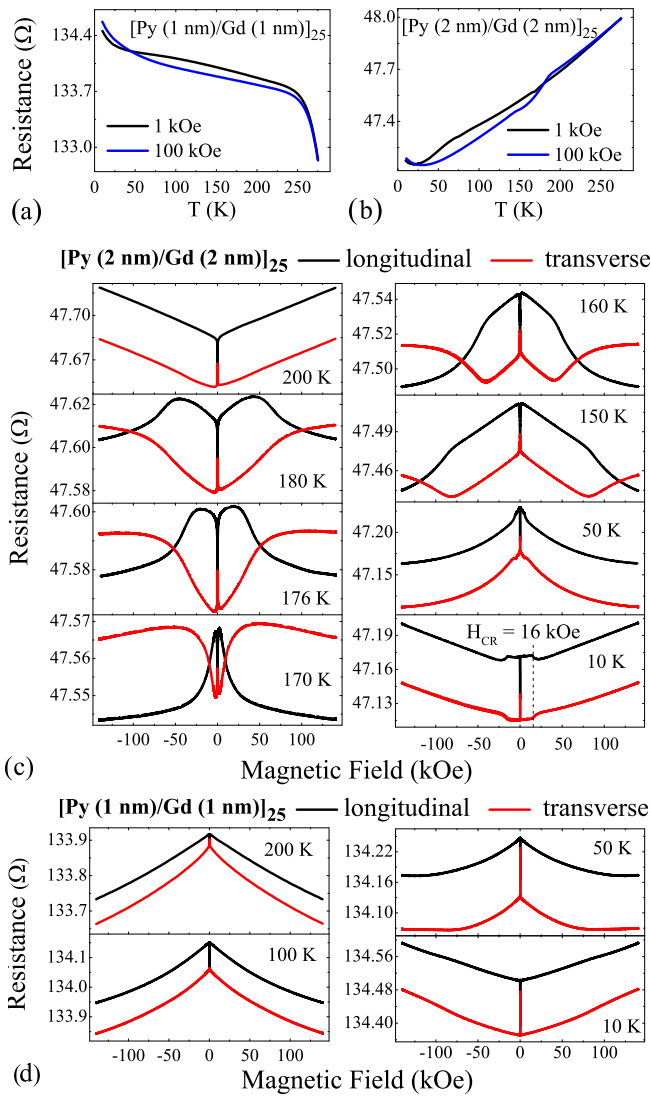**[Py (1 nm)/Gd (1 nm)]$_{25}$** —— longitudinal —— transverse

(d)

FIG. 4. Temperature dependences of the resistance measured in 1 kOe (black line) and 100 kOe (blue line) longitudinal magnetic fields for the (a) [Py (1 nm)/Gd (1 nm)]$_{25}$ and (b) [Py (2 nm)/Gd (2 nm)]$_{25}$ films. Resistance of the (c) [Py (2 nm)/Gd (2 nm)]$_{25}$ and (d) [Py (1 nm)/Gd (1 nm)]$_{25}$ films as a function of longitudinal (black line) and transverse (red line) magnetic fields.

structure is broken near the top and bottom surfaces of the [Py (2 nm)/Gd (2 nm)]$_{25}$ film. This causes the magnetizations near these surfaces to be at smaller angles with respect to the magnetic field than the magnetization inside the multilayer. To some extent, this configuration is similar to the twisted state predicted by Camley and Tilley [16], Camley [38], Jian [39], and Camley [40].

Although the simulated and experimental magnetization curves at 176 K demonstrate very similar behavior, they do not allow us to determine conclusively the magnetic configuration of the [Py (2 nm)/Gd (2 nm)]$_{25}$ film in the vicinity of the compensation temperature. Electronic transport measurements, on the other hand, are more sensitive to the distribution of the magnetization inside the films and its response to the applied magnetic field. Figure 4

demonstrates the results of transport measurements for both [Py (1 nm)/Gd (1 nm)]$_{25}$ and [Py (2 nm)/Gd (2 nm)]$_{25}$ films conducted for different magnetic fields and temperatures. First, Fig. 4(a) shows the temperature dependences of the resistance for the [Py (1 nm)/Gd (1 nm)]$_{25}$ film measured in the 1 kOe (black line) and 100 kOe (blue line) magnetic fields applied longitudinally. These measurements show that the magnetoresistance changes sign at around 40 K. Indeed, Fig. 4(d) illustrates that both longitudinal and transverse magnetoresistances are negative at 50 K, while they are positive at 10 K. Second, the same temperature [Fig. 4(b)] and magnetic-field [Fig. 4(c)] dependences for the [Py (2 nm)/Gd (2 nm)]$_{25}$ film indicate that the magnetoresistance changes the sign twice: around 20 K and, surprisingly, in the vicinity of the compensation temperature. Again, the magnetoresistance is positive at 200 K. In the vicinity of the compensation temperature, the magnetization rotates with respect to the magnetic film and the current, which leads to a change in the anisotropic magnetoresistance. Within the 150–180 K temperature range, a transverse resistance starts to increase while the longitudinal resistance starts to decrease when the amplitude of the magnetic field is increased. Similarly to the [Py (1 nm)/Gd (1 nm)]$_{25}$ film, the magnetoresistance of the [Py (2 nm)/Gd (2 nm)]$_{25}$ film is negative at 50 K and becomes positive again at 10 K.

The anisotropic magnetoresistance is responsible for an interesting steplike change in the resistance observed at 10 K in a 16 kOe magnetic field [Fig. 4(c)]. For the longitudinal resistance, it is an increase, and for the transverse resistance, it is a decrease. These steps are an additional evidence that the magnetization of the very bottom Py layer rotates and aligns along the magnetic field. This rotation provides a rise of the magnetization at 10 K for a 16 kOe magnetic field [Figs. 2(b) and 2(c)], as discussed previously. Similar changes of the resistance related to the nucleation of an in-plane domain wall have been reported previously for Fe/Gd [31,32] and Co/Gd [33] systems.

To define the orientation of the magnetizations in the [Py (2 nm)/Gd (2 nm)]$_{25}$ multilayer and to disentangle the contribution of the anisotropic magnetoresistance from that of the ordinary and giant magnetoresistances, we measured the angular dependences of the resistance in different magnetic fields. The idea is that, due to the anisotropic magnetoresistance, the resistance of the stripe reaches a minimum when the magnetizations in the layers are perpendicular to the direction of the current flow. As an example, the angular dependences of the resistance measured in a 10 kOe magnetic field at 174 and 176 K have minima at 90° and 87°, respectively (Fig. 5). Consequently, the magnetizations in the multilayer are parallel to the 10 kOe magnetic field at 174 and 176 K (collinear configuration). When the magnitude of the magnetic field is increased, the minima begin to shift. This indicates that the magnetization in the Gd-core/Mix and Py-core sublayers rotates with respect to the applied magnetic field. In a 30 kOe magnetic field, the minimum is at 52° at 174 K, and at 15° at 176 K. Hence, at 174 and 176 K, the angles between the magnetization and the 30 kOe magnetic field are 38° and 75°, respectively. The curves measured in a 70 kOe magnetic field have minima at around 0°; hence, the magnetizations are almost perpendicular to the magnetic field. It is noteworthy that the shape of some angular dependences is not completely
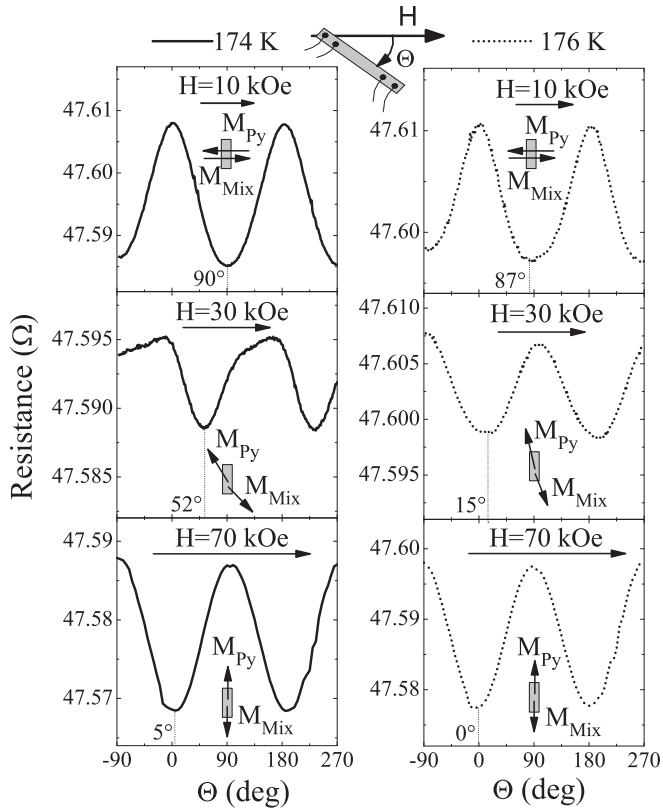
FIG. 5. Angular dependences of the resistance for the [Py (2 nm)/Gd (2 nm)]$_{25}$ multilayer measured at 174 and 176 K in 10, 30, and 70 kOe magnetic fields. The top central insert demonstrates the direction of the stripe rotation. A zero angle corresponds to a position where the long edge of the stripe is along the magnetic field. The small insets near each curve depict the orientations of the magnetizations in the Py-core (M_{Py}) and Mix (M_{Mix}) sublayers when the valve is at a 90° position.
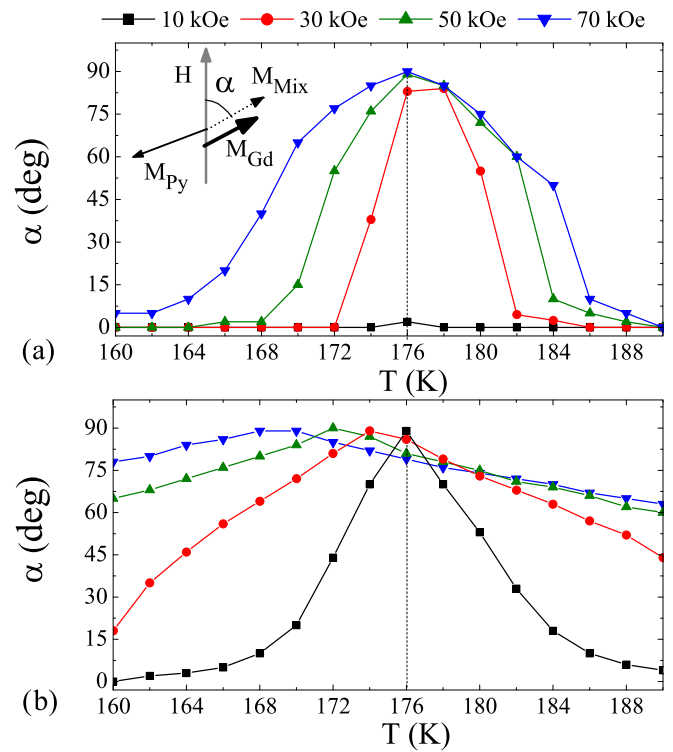

FIG. 6. (a) Experimental and (b) simulated temperature dependences of the angle between magnetic field and a line along which the magnetizations in the [Py (2 nm)/Gd (2 nm)]$_{25}$ film are predominantly aligned.

sinusoidal, and the amplitude of the angle-dependent parts of the curves are different at different temperatures. For example, at 174 K, this amplitude is 23 mΩ in 10 kOe, 7 mΩ in 30 kOe, and 19 mΩ in 70 kOe. This behavior can be attributed to a formation of a domain structure. The magnetizations in different domains can be mirrored with respect to the magnetic field. The averaging of the resistance produced by different domains may cause the reduction in the anisotropic magnetoresistance.

To map directions of magnetizations at different temperatures and magnetic fields, the angular dependences of the resistance were measured in 10, 30, 50, and 70 kOe magnetic fields in the 160–190 K temperature range. Then based on the positions of the resistance minima, the angle α between the magnetic field H and the axis along which the magnetizations in the Gd-core/Mix and Py-core sublayers are aligned was obtained [Fig. 6(a)]. The same $\alpha(H,T)$ dependence was modeled micromagnetically [Fig. 6(b)]. The most striking and unexpected result provided by the experimental dependence [Fig. 6(a)] is that, in a 10 kOe magnetic field, the collinear magnetization configuration is stable even at the compensation temperature, and the noncollinear magnetization configuration appears only in higher magnetic fields. The transition from the collinear magnetization configuration to the noncollinear

one does not produce any features in the magnetization curve measured at 176 K [Fig. 2(b) 176 K curve]. Additionally, in contrast to the simulations, the experimental $\alpha(H,T)$ dependence is very narrow (Fig. 6). In the experiment, the noncollinear configuration disappears in a 70 kOe magnetic field at temperatures 15 K above or below the compensation temperature.

The unusual phenomena observed in the vicinity of the compensation temperature for the [Py (2 nm)/Gd (2 nm)]$_{25}$ multilayer, namely the change in the magnetoresistance sign, the existence of transition from collinear to noncollinear configurations, and the unexpectedly narrow $\alpha(H,T)$ dependence, can be explained by an inhomogeneous sample structure. For modeling the magnetization of the [Py (2 nm)/Gd (2 nm)]$_{25}$ multilayer, we assumed that the magnetic and atomic structures of the film can be represented as a combination of the Mix, Py-, and Gd-core sublayers, and the thicknesses of these sublayers are the same throughout the film. However, it is possible that the accumulating roughness may very well change the amount of the intermixing and may result in the top layers of the [Py (2 nm)/Gd (2 nm)] multilayer more resembling the PyGd alloy. In this case, it is conceivable that the magnetization in this top part is Gd aligned even above 176 K, while the magnetization in the bottom part of the film is still Py aligned. Then above 176 K, one can expect an in-plane domain wall somewhere inside the film. An increase in the external magnetic field makes this domain wall narrower, which leads to an increase in the scattering, and consequently, the positive magnetoresistance. Second, the compensation observed at

176 K is not due to the equality of magnetic moments of the Mix/Gd-core and Py-core sublayers. The compensation occurs because the Gd-aligned magnetic moment of strongly intermixed top part of the film becomes equal to the Py-aligned magnetic moment of its bottom part. This yields the $\alpha(H,T)$ dependence to become narrow as it is observed in the experiment. Additionally, such different thickness-dependent intermixing may result in a thickness-dependent variation of the compensation temperature, which in turn would explain the remaining nonzero magnetization even at the experimentally observed compensation temperature.

We believe that the change in magnetoresistance sign at low temperatures for both [Py (2 nm)/Gd (2 nm)]$_{25}$ and [Py (1 nm)/Gd (1 nm)]$_{25}$ films is caused by the same mechanism. We do not expect that this sign change is due to an in-plane domain wall. First, based on the magnetic-field dependence of the resistance for the [Py (2 nm)/Gd (2 nm)]$_{25}$ film at 10 K [Fig. 4(c)], the magnetoresistance is positive even in magnetic fields lower than the nucleation field of the domain wall attributed to rotation of the magnetization in the first Py layer. Additionally, we do not expect nucleation of any in-plane domain wall in the [Py (1 nm)/Gd (1 nm)]$_{25}$ film. It is noteworthy a similar change in magnetoresistance sign was observed in a GdNi alloy [41], where it was speculated that the effect can be related to magnetic polarons induced by Gd.

V. EFFECTIVE EXCHANGE STIFFNESS

Based on the analysis of the temperature dependence of magnetization, we concluded that the Gd-core sublayers become ferromagnetic only below 75 K [Fig. 2(a)]. We expected that only a short-range exchange exists in the Gd-core sublayers above this temperature. This assumption is then implicitly used for simulating magnetization curve at the compensation temperature when we used $A_{Gd} = 0.1 \times 10^{-7}$ erg/cm. It is peculiar that the magnetic order inside the Gd layers can change so significantly on the scale of 2 nm. To investigate this effect more systematically, we fabricated Py (50 nm)/[Py (t)/Gd (t)]$_{25}$, $t = 1$ or 2 nm, films and studied how the effective exchange stiffness of the [Py (t)/Gd (t)]$_{25}$ stacks changes upon temperature increase. The total magnetic moment of the [Py (t)/Gd (t)]$_{25}$ stacks is Gd aligned below 275 K for $t = 1$ nm and below 176 K for $t = 2$ nm. Due to the antiferromagnetic coupling, this moment tends to be antiparallel to the magnetic moment of the 50-nm-thick Py layer adjacent to the stack. Since the effective exchange stiffness of the stack is expected to be much smaller than that for Py, applying magnetic field leads to an exchange-springlike rotation of the magnetization in the entire stack, and its total magnetic moment aligns along the magnetic field. Figures 7(a) and 7(b) illustrate the magnetization distribution over the thickness of the Py (50 nm)/[Py (2 nm)/Gd (2 nm)]$_{25}$ film at 10 K in high and low magnetic fields, respectively. As a model, the entire [Py (t)/Gd (t)]$_{25}$ stack can be considered as a homogeneous layer with some effective exchange stiffness A_{GdPy}. This effective layer is antiferromagnetically coupled to the 50-nm-thick Py layer. Applying the model for fitting the experimental magnetization curves of the Py (50 nm)/[Py (t)/Gd (t)]$_{25}$ film enables estimating A_{GdPy} at different temperatures. The analysis shows that, at 10 K, the Py/Gd stacks of both films can be
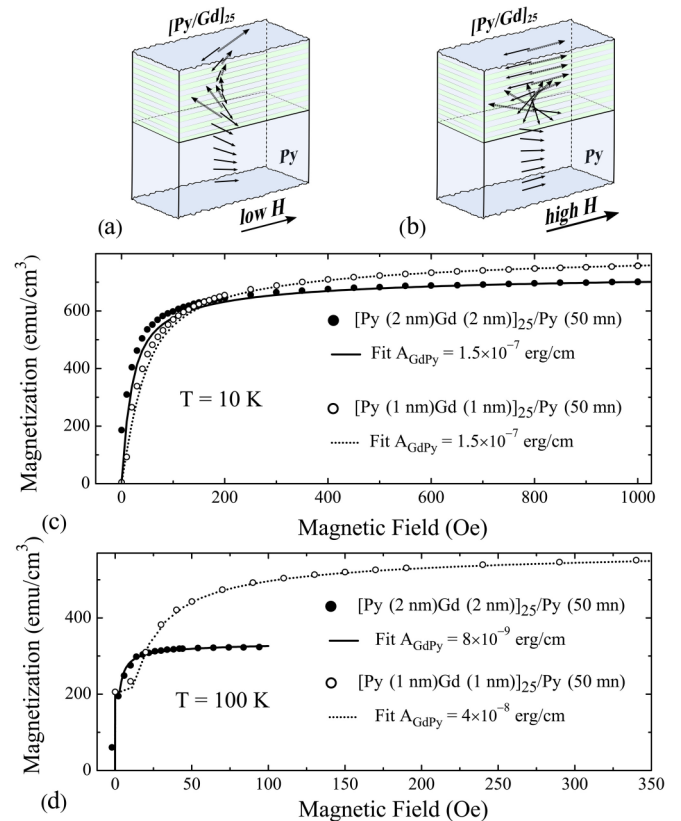

FIG. 7. The in-plane domain walls in Py (50 nm)/[Py (2 nm)/ Gd (2 nm)]$_{25}$ in (a) high and (b) low magnetic fields. Magnetization curves of Py (50 nm)/[Py (2 nm)/Gd (2 nm)]$_{25}$ (solid circles = experimental data; solid lines = fits) and Py (50 nm)/[Py (1 nm)/ Gd (1 nm)]$_{25}$ (open circles = experimental data; dotted line = fits) at (c) 10 K and (d) 100 K.

characterized by the same effective exchange stiffness $A_{GdPy} = 1.5 \times 10^{-7}$ erg/cm. At 100 K, the effective exchange stiffness of the [Py (1 nm)/Gd (1 nm)]$_{25}$ stack becomes equal to 4×10^{-8} erg/cm, while that for the [Py (2 nm)/Gd (2 nm)]$_{25}$ stack is five times smaller (8×10^{-9} erg/cm). This observation proves that the inner portions of the Gd layers have lower exchange stiffness, and the Py layers are responsible for the enhancement of the magnetic order in the Gd layers.

VI. CONCLUSIONS

Analysis of the magnetization curves for the Py/Gd bilayers shows that, due to proximity with Py, the magnetic order of about 1 nm of the Gd layer adjacent to the Py layer is strongly enhanced. Micromagnetic simulations demonstrate that the magnetization reversal observed in the Py (50 nm)/Gd (4 nm) bilayers in 1.3 kOe is due to an exchange-springlike twisting of the magnetization in the Gd layer. The exchange stiffness of the Gd layer and, hence, parameters of the twist can be controlled by inserting an ultrathin layer of Au between Py and Gd. Using a combination of magnetometry and magnetotransport measurements, we determined the magnetic structures of the Py/Gd multilayers. Based on the reduction of the Curie temperature, it was concluded that the [Py (1 nm)/Gd (1 nm)]$_{25}$ film is mostly composed of a PyGd alloy. The [Py (2 nm)/Gd (2 nm)]$_{25}$ film

has a complex magnetic structure. Based on the magnetometry data, it was estimated that the 0.5-nm-thick inner portions of the Py and Gd layers are not affected by intermixing. Analysis of the angular dependences of resistance for this film revealed that a noncollinear magnetization configuration is only stable in an unexpectedly narrow range of temperatures, and there is a transition from the collinear to noncollinear configurations at 10 kOe magnetic field, even at the compensation temperature. We believe that the unusual behavior at the compensation temperature is due to accumulative roughness which causes the structure of the [Py (2 nm)/Gd (2 nm)]$_{25}$ multilayer to be inhomogeneous over its thickness. Hence, different parts of the film can be characterized by different compensation temperatures, and the minimum of the film magnetization observed at 176 K occurs due to an equality of the magnetic moments in the majority of the film. The inhomogeneity may also be responsible for the appearance of the in-plane domain wall in the film at temperatures above 176 K, which results in

the change in the magnetoresistance sign at the compensation temperature. A more complicated model which takes into account accumulative roughness is required in order to model the phenomena micromagnetically. We believe that intermixing and accumulative roughness may affect magnetization behavior at the compensation temperature for other artificial ferrimagnets as well. Analysis of the magnetization curves for the Py (50 nm)/[Py (t)/Gd (t)]$_{25}$ multilayers, where t is 1 or 2 nm, demonstrates that, above 75 K, the exchange stiffness inside the Gd layers is reduced and the magnetic order changes drastically on the scale of 2 nm.

[1] R. Wu and A. J. Freeman, J. Magn. Magn. Mater. **99**, 81 (1991).

[2] A. Heys, P. E. Donovan, A. K. Petford-Long, and R. Cywinski, J. Magn. Magn. Mater. **131**, 265 (1994).

[3] A. Heys and P. E. Donovan, J. Magn. Magn. Mater. **126**, 326 (1993).

[4] D. Weller, S. F. Alvarado, W. Gudat, K. Schröder, and M. Campagna, Phys. Rev. Lett. **54**, 1555 (1985).

[5] A. Barth, F. Treubel, M. Marszałek, W. Evenson, O. Hellwig, C. Borschel, M. Albrecht, and G. Schatz, J. Phys.: Condens. Matter **20**, 395232 (2008).

[6] M. Taborelli, R. Allenspach, G. Boffa, and M. Landolt, Phys. Rev. Lett. **56**, 2869 (1986).

[7] D. Haskel, G. Srajer, J. C. Lang, J. Pollmann, C. S. Nelson, J. S. Jiang, and S. D. Bader, Phys. Rev. Lett. **87**, 207201 (2001).

[8] J. W. A. Robinson, F. Chiodi, M. Egilmez, G. B. Halász, and M. G. Blamire, Sci. Rep. **2**, 699 (2012).

[9] T. Katayama, M. Hirano, Y. Koizumi, K. Kawanishi, and T. Tsushima, IEEE Trans. Magn. **13**, 1603 (1977).

[10] M. Nawate, K. Doi, and S. Honda, J. Magn. Magn. Mater. **126**, 279 (1993).

[11] T. Eimüller, R. Kalchgruber, P. Fischer, G. Schütz, P. Guttmann, G. Schmahl, M. Köhler, K. Prügl, M. Scholz, F. Bammes, and G. Bayreuther, J. Appl. Phys. **87**, 6478 (2000).

[12] S. Tomonori, O. Kouji, O. Kenshou, O. Yutaka, M. Shunsuke, and S. Yoshifumi, Jpn. J. Appl. Phys. **13**, 201 (1974).

[13] J. C. T. Lee, J. J. Chess, S. A. Montoya, X. Shi, N. Tamura, S. K. Mishra, P. Fischer, B. J. McMorran, S. K. Sinha, E. E. Fullerton, S. D. Kevan, and S. Roy, Appl. Phys. Lett. **109**, 022402 (2016).

[14] S. Woo, K. M. Song, X. Zhang, Y. Zhou, M. Ezawa, S. Finizio, J. Raabe, J. W. Choi, B.-C. Min, H. C. Koo, and J. Chang, arXiv:1703.10310.

[15] S. A. Montoya, S. Couture, J. J. Chess, J. C. T. Lee, N. Kent, D. Henze, S. K. Sinha, M. Y. Im, S. D. Kevan, P. Fischer, B. J. McMorran, V. Lomakin, S. Roy, and E. E. Fullerton, Phys. Rev. B **95**, 024415 (2017).

[16] R. E. Camley and D. R. Tilley, Phys. Rev. B **37**, 3413 (1988).

[17] C. D. Stanciu, F. Hansteen, A. V. Kimel, A. Kirilyuk, A. Tsukamoto, A. Itoh, and T. Rasing, Phys. Rev. Lett. **99**, 047601 (2007).

[18] S. Mangin, M. Gottwald, C. H. Lambert, D. Steil, V. Uhlíř, L. Pang, M. Hehn, S. Alebrand, M. Cinchetti, G. Malinowski, Y. Fainman, M. Aeschlimann, and E. E. Fullerton, Nat. Mater. **13**, 286 (2014).

[19] T. A. Ostler, J. Barker, R. F. L. Evans, R. W. Chantrell, U. Atxitia, O. Chubykalo-Fesenko, S. El Moussaoui, L. Le Guyader, E. Mengotti, L. J. Heyderman, F. Nolting, A. Tsukamoto, A. Itoh, D. Afanasiev, B. A. Ivanov, A. M. Kalashnikova, K. Vahaplar, J. Mentink, A. Kirilyuk, T. Rasing, and A. V. Kimel, Nat. Commun. **3**, 666 (2012).

[20] A. Kirilyuk, A. V. Kimel, and T. Rasing, Rep. Prog. Phys. **76**, 026501 (2013).

[21] C. Xu, T. A. Ostler, and R. W. Chantrell, Phys. Rev. B **93**, 054302 (2016).

[22] C.-H. Lambert, S. Mangin, B. S. D. C. S. Varaprasad, Y. K. Takahashi, M. Hehn, M. Cinchetti, G. Malinowski, K. Hono, Y. Fainman, M. Aeschlimann, and E. E. Fullerton, Science **345**, 1337 (2014).

[23] R. Morales, J. I. Martín, and J. M. Alameda, Phys. Rev. B **70**, 174440 (2004).

[24] C. Blanco-Roldán, Y. Choi, C. Quirós, S. M. Valvidares, R. Zarate, M. Vélez, J. M. Alameda, D. Haskel, and J. I. Martín, Phys. Rev. B **92**, 224433 (2015).

[25] S. Honda, M. Nawate, and I. Sakamoto, J. Appl. Phys. **79**, 365 (1996).

[26] R. Ranchal, C. Aroca, M. Maicas, and E. López, J. Appl. Phys. **102**, 053904 (2007).

[27] R. Ranchal, C. Aroca, and E. López, J. Appl. Phys. **100**, 103903 (2006).

[28] R. Ranchal, Y. Choi, M. Romera, J. W. Freeland, J. L. Prieto, and D. Haskel, Phys. Rev. B **85**, 024403 (2012).

[29] The code is available at http://math.nist.gov/oommf.

[30] L. T. Baczewski, R. Kalinowski, and A. Wawro, J. Magn. Magn. Mater. **177-181**, 1305 (1998).

[31] M. Vaezzadeh, B. George, and G. Marchal, Phys. Rev. B **50**, 6113 (1994).

[32] K. Takanashi, Y. Kamiguchi, H. Fujimori, and H. Motokawa, J. Phys. Soc. Jpn. **61**, 3721 (1992).

[33] J. Colino, J. P. Andrés, J. M. Riveiro, J. L. Martínez, C. Prieto, and J. L. Sacedón, Phys. Rev. B **60**, 6678 (1999).

[34] K. Takanashi, H. Kurokawa, and H. Fujimori, Appl. Phys. Lett. **63**, 1585 (1993).

[35] D. LaGraffe, P. A. Dowben, and M. Onellion, J. Vac. Sci. Technol. A **8**, 2738 (1990).

[36] T. McGuire and R. Gambino, IEEE Trans. Magn. **14**, 838 (1978).

[37] R. Ranchal, C. Aroca, M. Sánchez, P. Sánchez, and E. López, Appl. Phys. A **82**, 697 (2006).

[38] R. E. Camley, Phys. Rev. B **35**, 3608 (1987).

[39] Y. Jian, Solid State Commun. **74**, 1221 (1990).

[40] R. E. Camley, Phys. Rev. B **39**, 12316 (1989).

[41] R. Mallik, E. V. Sampathkumaran, P. L. Paulose, and V. Nagarajan, Phys. Rev. B **55**, R8650(R) (1997).